Molecular Cell
Article

Differences in the Mechanisms of Proapoptotic BH3 Proteins Binding to Bcl-XL and Bcl-2 Quantified in Live MCF-7 Cells

Alexander Aranovich,[1,3] Qian Liu,[1,3] Tony Collins,[1] Fei Geng,[1] Sudeepa Dixit,[1] Brian Leber,[1,2] and David W. Andrews[1,*]
[1]Department of Biochemistry and Biomedical Sciences
[2]Department of Medicine
McMaster University, Hamilton, ON L8N 3Z5, Canada
[3]These authors contributed equally to this work
*Correspondence: andrewsd@dwalab.ca
DOI 10.1016/j.molcel.2012.01.030

SUMMARY

Overexpression of antiapoptotic proteins including Bcl-XL and/or Bcl-2 contributes to tumor initiation, progression, and resistance to therapy by direct interactions with proapoptotic BH3 proteins. Release of BH3 proteins from antiapoptotic proteins kills some cancer cells and sensitizes others to chemotherapy. Binding of Bcl-XL and Bcl-2 to the BH3 proteins Bad, Bid, and the three major isoforms of Bim was measured for fluorescent protein fusions in live cells using fluorescence lifetime imaging microscopy and fluorescence resonance energy transfer. In cells the binding of the proteins at mitochondria is similar to the results from in vitro measurements. However, mutations in the BH3 region of Bim known to inhibit binding to Bcl-XL and Bcl-2 in vitro had much less effect in MCF-7 cells. Moreover, the BH3 mimetic ABT-737 inhibited Bad and Bid but not Bim binding to Bcl-XL and Bcl-2. Thus, the selectivity of ABT-737 also differs markedly from predictions made from in vitro measurements.

INTRODUCTION

Apoptosis is a programmed cell death process involved in development, homeostasis, and immune defense in multicellular organisms. Mitochondrial outer membrane permeabilization commits the cell to apoptosis and is regulated by direct physical interactions between the proapoptotic proteins Bax and Bak; the antiapoptotic proteins Bcl-2, Bcl-XL, and Mcl-1; and the BH3 proteins that activate Bax and Bak (Activators) and/or inhibit the antiapoptotic proteins (Sensitizers) (Youle and Strasser, 2008).

Tumor cell survival often depends upon the antiapoptotic activity of Bcl-2, Bcl-XL, and/or Mcl-1 restraining the proapoptotic proteins that are activated in tumor cells (Certo et al., 2006). For example, overexpression of Bcl-XL has been found in many cancers where it contributes to tumor initiation, progression, and resistance to therapy (Kirkin et al., 2004). Thus, inhibition of antiapoptotic proteins is expected to either selectively kill or sensitize cancer cells to chemotherapy. As a result there has been a major effort to understand how BH3 proteins bind to Bcl-2 and Bcl-XL as well as to discover or design small-molecule inhibitors of these antiapoptotic proteins.

Here we examined the binding of both sensitizer (Bad) and activator (Bid, Bim) BH3 proteins to Bcl-XL and Bcl-2, two of the most abundantly expressed antiapoptotic proteins. As Bid is activated by cleavage, we measured binding after inducing cleavage by treating the cells with an apoptotic agonist or by expressing a truncated, constitutively active form of the protein. We also measured binding of BimEL and BimL (the two most widely expressed isoforms) and BimS (a rarely expressed but highly potent splice variant) to Bcl-2 and Bcl-XL.

One of the most successful inhibitors of both Bcl-2 and Bcl-XL is ABT-737, a mimetic of the BH3 protein Bad interacting with Bcl-XL (Oltersdorf et al., 2005; Bruncko et al., 2007). ABT-737 binds with high affinity ($K_i \leq 1$ nM) to the soluble domains of Bcl-XL, Bcl-2, and Bcl-w in vitro and displaces BH3 peptides derived from both activator (e.g., Bid and Bim) and sensitizer (e.g., Bad) BH3 proteins from this domain of Bcl-XL. The cytotoxic activity of the compound is lost in cells deficient for Bax and Bak or caspase-9, demonstrating its specificity (Vogler et al., 2009). ABT-737 exhibits minimal in vitro and in vivo activity toward normal cells, while it is toxic to some transformed cells (Hann et al., 2008; Chauhan et al., 2007; Oltersdorf et al., 2005). The precise mechanistic specificity of ABT-737 in live cells is not known and has only been inferred from indirect measures in cells and animals (Mason et al., 2008) or measurements made in vitro using protein fragments and/or peptides.

The relative affinity of the interactions between Bcl-2 family proteins depends to a large extent on whether the proteins interact in the cytoplasm or in cellular membranes (Leber et al., 2007, 2010). The structural changes that result when the proteins insert into membranes led to dramatic changes in interacting partners. For example, the caspase-8 cleaved form of the BH3 protein Bid did not bind to Bax in solution, yet bound tightly to and activated the protein in membranes (Lovell et al., 2008). Thus, it is challenging to extrapolate measurements of binding interactions made in vitro using soluble truncated forms of the proteins and peptides (Chen et al., 2005; Giam et al., 2008) to what happens in live cells.

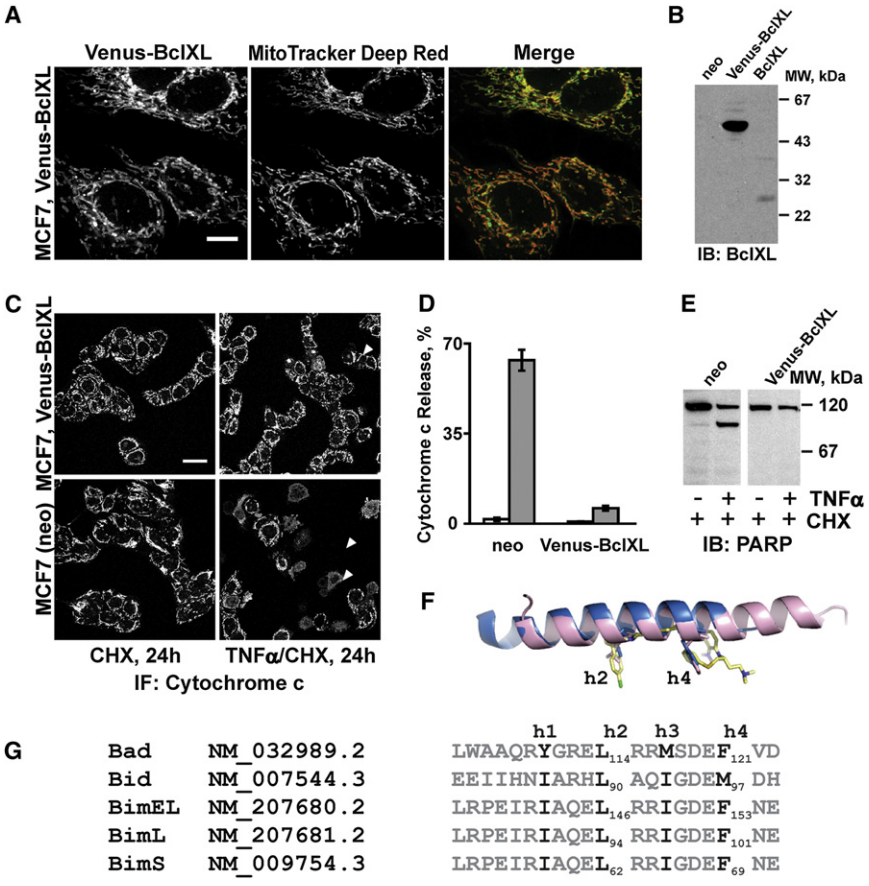

Figure 1. Characterization of MCF-7 Expressing Venus-Bcl-XL

(A) Venus-Bcl-XL localizes partly to mitochondria. Representative cells illustrating colocalization of Venus-Bcl-XL with MitoTracker Deep Red on mitochondria. Scale bar is 10 μm.

(B) Comparative expression level and sizes of Bcl-XL in MCF-7 cell lines stably transfected with empty (neo), Venus-Bcl-XL, and Bcl-XL vectors.

(C–E) MCF-7 cell lines stably expressing Venus-Bcl-XL are resistant to apoptotic events downstream of Bid cleavage in response to TNF-α/CHX treatment. Representative confocal images of cells immunostained for cytochrome *c* after being treated for 24 hr with CHX or TNF-α/CHX (C); arrowheads indicate some of the cells with released cytochrome *c*. Scale bar 25 μm. The fraction of cells with diffuse cytochrome *c* staining manually counted for more than 450 cells from three independent experiments (±SD) (D); cells treated with CHX or TNF-α/CHX, white and gray bars, respectively. PARP cleavage in MCF-7 cells stably transfected with empty (neo) or Venus-Bcl-XL constructs treated for 24 hr with TNF-α/CHX (E); the migration position of molecular weight markers (MW) is indicated to the right.

(F) Structural alignment of BH3 peptides with ABT-737 from the complexes: Bcl-XL:Bim-BH3 (1PQ1, pink), Bcl-XL:Bad-BH3 (2BZW, blue), and Bcl-XL:ABT-737 (2YXJ, yellow). ABT-737 and side chains of the key hydrophobic residues (h2 and h4) in the BH3 peptides are shown and labeled.

(G) Sequence alignments for the BH3 regions from the indicated proteins. The conserved hydrophobic residues (h1–h4) are bolded. Residue numbers of h2 and h4 that were mutated to alanine in the 2A mutants are labeled as subscripts. See also Figure S1.

To measure the interactions of Bcl-XL and Bcl-2 with the proapoptotic BH3 proteins in live cells, the antiapoptotic proteins were expressed as fusions to the yellow fluorescence protein Venus, and the proapoptotic BH3 proteins including Bid (Wang et al., 1996), Bim (O'Connor et al., 1998; Bouillet et al., 1999), and Bad (Yang et al., 1995) were fused to the red fluorescence protein mCherry. As about half of the cellular Bcl-XL is normally cytoplasmic, interactions were visualized by monitoring the redistribution of the protein from the cytoplasm to mitochondria. Direct binding was quantified using fluorescence lifetime imaging microscopy (FLIM) to measure fluorescence resonance energy transfer (FRET) (Chen et al., 2003; Chen and Periasamy, 2004; Periasamy and Day, 2005). Interactions between Bcl-XL and BH3 proteins bring Venus (donor) and mCherry (acceptor) less than 100 Å apart (Shaner et al., 2004; Zacharias et al., 2002), resulting in FRET that can be detected as a decrease in the fluorescence lifetime of Venus-Bcl-XL.

Energy transfer measurements allowed us to gauge the relative affinity of Bcl-2 family protein interactions in live cells. Our data show that ABT-737 inhibits the binding of tBid and Bad, but surprisingly, not the major isoforms of Bim, to both Bcl-XL and Bcl-2. Consistent with this result, mutations in the conserved BH3 region dramatically reduced binding of Bad and tBid, but not the three isoforms of Bim, to the membrane-bound forms of either Bcl-XL or Bcl-2, suggesting that in live cells Bim interacts with these molecules by additional interactions that may be outside of the BH3 region. Neither result could have been inferred from previous in vitro measurements. Clearly, FLIM FRET provides unique information regarding the interactions of proteins in live cells. The ability to measure protein:protein interactions in live cells is expected to provide insights into many other systems and is likely to guide future efforts to change the specificity or mechanism of drugs like ABT-737.

RESULTS

Venus-Antiapoptotic Proteins and mCherry-BH3 Proteins Function in MCF-7 Cells

To measure the interactions in live cells between Bcl-2 and Bcl-XL with the sensitizer BH3 protein Bad and the activator BH3 proteins tBid and three Bim isoforms, plasmids were constructed that expressed the proteins as fluorescence protein fusions. Bcl-XL and Bcl-2 were stably expressed in the breast cancer cell line MCF-7 with the yellow fluorescence protein Venus fused at the N terminus. Similar to the untagged protein, some Venus-Bcl-XL colocalized with Mitotracker Deep Red, confirming that it localized at mitochondria (Figure 1A). Increasing the intensity in the images revealed that in nonmitochondrial areas

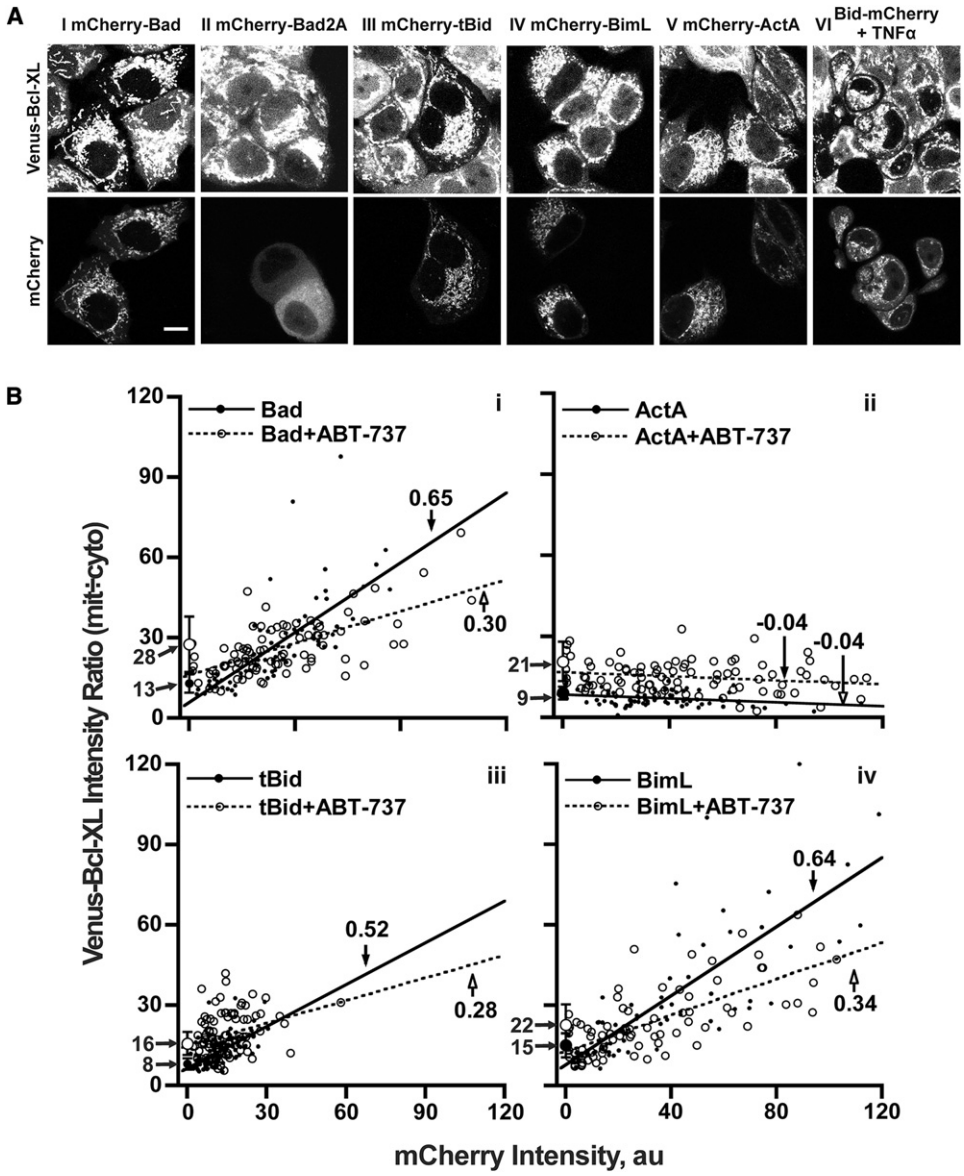

Figure 2. BH3 Proteins and ABT-737 Trigger Redistribution of Cytoplasmic Venus-Bcl-XL to Mitochondria in MCF-7 Cells

(A) Electronically amplified (beyond saturation) signal in confocal micrographs revealed Venus-Bcl-XL in both the cytoplasm and nuclear area. Expression of mCherry-BH3-only proteins, but not the controls mCherry-Bad2A and mCherry-ActA, resulted in redistribution of the Venus-Bcl-XL signal from the cytoplasm to mitochondria visualized as decreased intensity of the Venus-Bcl-XL in nonmitochondrial spaces such as the nucleus for cells expressing an mCherry-BH3 protein.

(B) Venus-Bcl-XL intensities (mit/cyto) versus total mCherry for individual cells fit to a straight line using linear regression. The positive slope of the lines is consistent with increased expression of mCherry-BH3 protein increasing the fraction of Venus-Bcl-XL at mitochondria (solid dots). Addition of ABT-737 increased the mit:cyto ratio of Venus-Bcl-XL approximately 2-fold for the untransfected (mCherry intensity = 0, arrows at the left; p values for t test $< 10^{-5}$ for all four panels). ABT-737 recruits Venus-Bcl-XL poorly, but competes with BH3 proteins for binding to cytoplasmic Venus-Bcl-XL, reducing the slope of the line of best fit for recruitment of Venus-Bcl-XL by BH3 proteins (open dots). See also Figure S2.

(e.g., nuclei) the average intensity of Venus-Bcl-XL was about 10% that of the signal at mitochondria, corresponding to about half of the Venus-Bcl-XL being located at mitochondria in untreated cells (Figure 2A). High-level expression of Venus-Bcl-XL ensured that there was little interference from the endogenous nonfluorescent protein in our assays, as the endogenous protein (not visible on the blot in Figure 1B, neo) was expressed at a very low level in these cells. Venus-Bcl-XL inhibited apoptosis induced by TNF-α and cycloheximide assessed as prevention of the release of cytochrome *c* from mitochondria (Figures 1C and 1D) and by inhibition of PARP cleavage (Figure 1E) and prevented apoptosis due to expression of either tBid or Bim by transient transfection (Galluzzi et al., 2009). Similarly, Bcl-2 fusion proteins with an N-terminal fluorescent protein have already been

shown functional in a variety of cell systems and therefore are not shown here (Renton et al., 2010). Thus, Venus-Bcl-XL and Venus-Bcl-2 retained antiapoptotic function in MCF-7 cells.

To visualize the BH3 proteins, they were expressed with either an N- (Bim, Bad, tBid) or C- (Bid) terminal mCherry fluorescent protein. In order to obtain a wide variation in the amount of the mCherry fusion proteins, they were expressed by transient transfection in MCF-7 cells. As expected, all of the mCherry-fusion proteins retained the expected cytochrome *c* release activity based on the known functions of the untagged proteins and were inhibited by Bcl-XL, demonstrating that the tagged versions function in live MCF-7 cells (Figure S1). As controls, two conserved hydrophobic residues in the BH3 region, which ABT-737 was designed to mimic, were replaced by alanine (2A mutations, Figures 1F and 1G). The 2A mutations abolished the function of tBid (as effectively as the well-characterized inactivating G94E mutation) and Bad, but the corresponding mutations in BimEL2A, BimL2A, and BimS2A remained proapoptotic and inhibitable by Bcl-XL (Figure S1). In contrast, these mutations effectively inhibited binding of all BH3 peptides to the cytoplasmic domain of Bcl-XL or Bcl-2 when measured in vitro (Lee et al., 2008; Schimmer et al., 2001; Peng et al., 2006).

BH3 Proteins and ABT-737 Trigger Redistribution of Bcl-XL to Mitochondria

Interactions between Bcl-2 family proteins expressed in cells cannot be usefully assayed by coprecipitation, as nonionic detergents artificially promote binding of the proteins (Hsu and Youle, 1998) while the zwitterionic detergent CHAPS artificially inhibits the interactions (Lovell et al., 2008). Therefore, we sought other methods to measure interactions between the proteins in live cells. Like Bcl-XL and unlike the constitutively transmembrane protein Bcl-2, Venus-Bcl-XL was found in both the cytoplasm and mitochondria of cells (Figure 2A). Transient expression of a BH3 protein resulted in redistribution of Venus-Bcl-XL to mitochondria that correlated with the expression level of the BH3-only protein. Redistribution is most easily visualized as a decrease in the Venus signal in the nuclei of cells expressing a BH3 protein (Figure 2A). By plotting localization at mitochondria versus intensity of the mCherry-BH3 protein, the slope of the line of best fit provides an indirect measure of the efficiency of the interaction between cytoplasmic Bcl-XL and the BH3 protein. Despite being quite noisy, the line of best fit for the redistribution data was similar for Bad, Bim, and tBid, suggesting that the different BH3 proteins bind to cytoplasmic Venus-Bcl-XL similarly (Figure 2B, i, iii, and iv). BH3 protein-mediated redistribution of Venus-Bcl-XL is consistent with our previous observations in vitro using full-length proteins (Billen et al., 2008). In contrast, expression of the control protein mCherryBad2A that does not bind Bcl-XL did not trigger redistribution of Venus-Bcl-XL (Figure 2A, ii). Furthermore, expression of mCherry-ActA, a control protein that does not bind to Venus Bcl-XL but in which mCherry is targeted directly to mitochondria via fusion to the mitochondria-specific Act-A tail-anchor sequence (Zhu et al., 1996), did not increase Venus-Bcl-XL at mitochondria. However, the slight decrease in binding at high expression levels of mCherry-ActA may indicate competition for a limited number of binding sites on mitochondria (Figure 2B, ii).

Addition of the BH3 mimetic compound ABT-737 also resulted in redistribution of cytoplasmic Venus-Bcl-XL to mitochondria, consistent with the compound functioning as a BH3 protein mimetic in live cells (compared quantitatively for cells in which the expression of mCherry-BH3 protein was undetectable in Figure 2B, points at located at "0 mCherry intensity" on the x axis). In control experiments, addition of ABT-737 resulted in redistribution of Venus-Bcl-XL to mitochondria (Figure S2A) in approximately 3 hr (Figure S2B).

At low expression of the BH3 protein, addition of the ABT-737 increased Bcl-XL redistribution to membranes. However, ABT-737 was less effective than BH3 proteins at mediating redistribution to membranes. As a result, in cells with higher expression of BH3 proteins, competition with ABT-737 reduced the binding of these BH3 proteins to cytoplasmic Bcl-XL. This decreases the efficiency of Bcl-XL redistribution, as shown by the reduced slope for the lines of best fit for all of the BH3 proteins (Figure 2B).

As the changes in slopes are statistically significant ($p < 0.05$), these redistribution measurements strongly suggest a mutually exclusive direct interaction between the BH3 proteins and ABT-737 with cytoplasmic Bcl-XL. However, the data are very noisy, making quantification difficult. Additional uncertainty was seen for measurements with tBid, because at higher expression levels, it caused the cells to round up and die, preventing accurate quantification (Figure S1). Furthermore, redistribution from cytoplasm to membranes cannot be used to assess binding of BH3 proteins to the membrane-bound form of Bcl-XL or to the constitutively membrane-bound Bcl-2. This is because colocalization is not sufficient to conclude that the proteins are bound to each other, as good colocalization was also observed when the control protein mCherry-ActA was expressed at mitochondria (Figure 2A, v).

Quantification of BH3 Protein Binding to Bcl-XL by FLIM FRET

To examine the binding of the sensitizer BH3 protein Bad to Bcl-XL, FLIM FRET was measured for mCherry-Bad binding to Venus-Bcl-XL (Figure 3). In FLIM FRET, changes in the fluorescence lifetime of a fluorescence protein that result when two fluorescence proteins are brought together by heterodimerization of their fusion partners are used to measure FRET in live cells. The decrease in Venus (donor) lifetime compared to appropriate controls can be used to measure protein:protein interactions in live cells robustly because, unlike other methods, FLIM is not affected by spectral bleed-through or by changes in the excitation intensity (Zacharias et al., 2002). As the distance between the donor and acceptor is fixed when they form a heterodimer, the extent of FRET (referred to as FLIM FRET efficiency) for any one donor-acceptor pair is a measure of the proportion of Venus-antiapoptotic protein bound to mCherry-BH3 protein in that pixel or region of interest in the image (Chen et al., 2003; Chen and Periasamy, 2004; Periasamy and Day, 2005). Thus, FLIM FRET can be used to measure changes in the binding of any individual pair of donor and acceptor proteins, but cannot be used to compare two different pairs, i.e., the absolute amount of binding of two different BH3 proteins cannot be compared, but the way their binding changes in response to a stimulus can be compared.

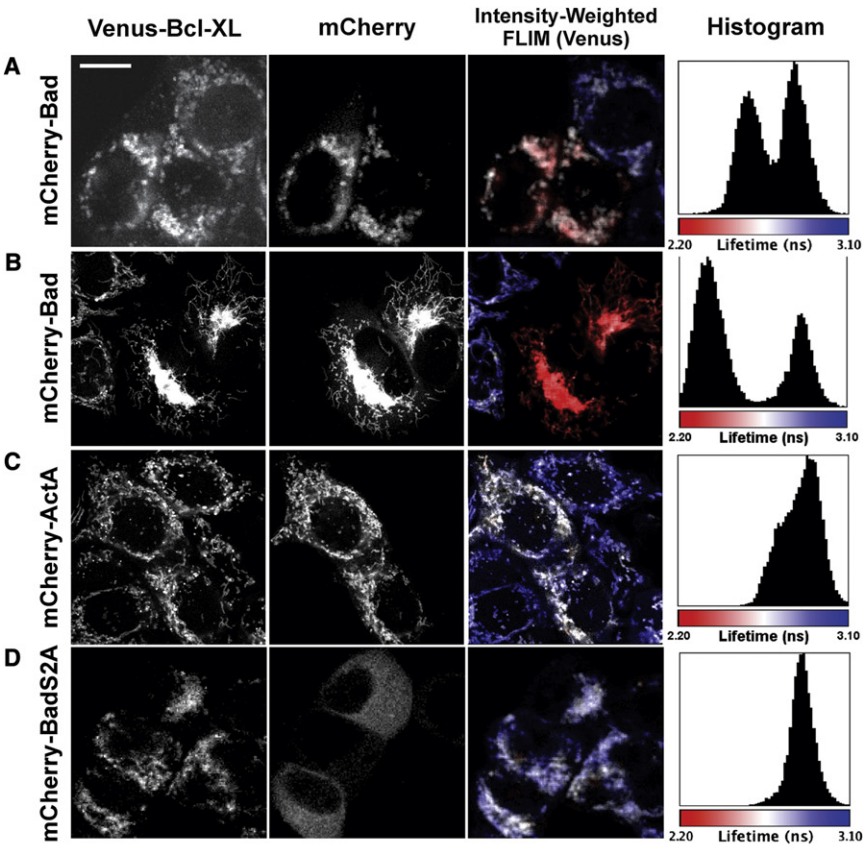

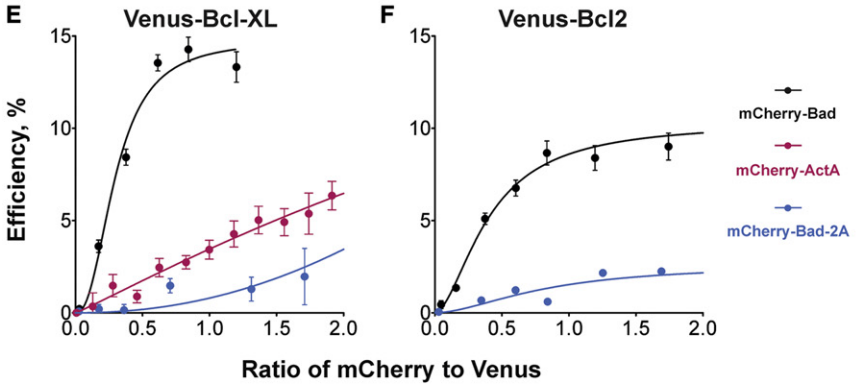

Figure 3. Binding of mCherry-Bad to Venus-Bcl-XL Measured in Live Cells using FLIM-FRET

(A–D) Intensity images of Venus-Bcl-XL (left) and mCherry (middle) and intensity-weighted FLIM images of Venus-Bcl-XL (right). Fluorescence lifetimes are presented in a continuous pseudocolor scale ranging from 2.2 to 3.1 ns. A histogram of Venus-Bcl-XL fluorescence lifetimes for image pixels is shown on the right using the same pseudocolor scale in which FRET is indicated by the red color. Scale bar is 10 μm. Live MCF-7 cells stably expressing Venus-Bcl-XL and transiently expressing mCherry-Bad (moderate expression, A), mCherry-Bad (high expression, B), the mitochondrial localized control protein mCherry-ActA (C), and the non-Bcl-XL-binding mutant mCherry-Bad2A (D).

(E and F) Curves illustrating binding of the indicated proteins to Venus-Bcl-XL (E) or Venus-Bcl-2 (F). Binding to mCherry-Bad (black), collisions between mCherry-ActA and Venus-Bcl-XL (red), and lack of binding of mCherry-Bad2A (blue) are shown. The FLIM FRET efficiency (Efficiency %), a measure of bound fraction for areas within individual cells expressing mCherry-Bad and Venus-Bcl-XL or Venus-Bcl-2 as indicated, was plotted versus the ratio of the steady-state intensity of mCherry to Venus fluorescence. Error bars, SE. Each curve > 450 cells. See also Figure S3.

Expression of mCherry-Bad in Venus-Bcl-XL-expressing cells resulted in significantly shorter Venus-Bcl-XL fluorescence lifetimes (2.56 ns; Figure 3A, red color in intensity-weighted images) compared to cells expressing only Venus-Bcl-XL (2.82 ns) in the same image. The distribution of the numerical values of different Venus-Bcl-XL lifetimes in individual pixels displayed as histograms for all of the cells in the image in Figure 3 was used to calculate an average FLIM FRET efficiency of 9.3% for these cells. Expression of a sensitizer BH3-protein like Bad is relatively noncytotoxic in the absence of a proapoptotic stimulus; as a result, some cells expressed very high levels of mCherry-Bad yet retained relatively normal morphology. In these cells more of the Venus-Bcl-XL was bound to mCherry-Bad, which increased FRET and resulted in an even shorter Venus-Bcl-XL lifetime (2.36 ns, FLIM FRET efficiency 17%) compared to 2.84 ns for the cells not expressing detectable mCherry-Bad in the same image (Figure 3B). These data demonstrate that the FLIM FRET efficiency is a measure of the binding of mCherry-Bad to Venus-Bcl-XL. It also suggests that FLIM FRET data for cells with a wide range of relative expression levels can be used to plot binding curves for these interacting proteins, as shown previously for other proteins (Zacharias et al., 2002).

When the two proteins were recruited to membranes, the number of collisions between them was expected to increase, because the local concentration is high and the rate of diffusion is low compared to when they are in cytoplasm. Both factors might increase the FRET detected due to random collisions. To determine the extent to which collisions between the proteins in the outer mitochondrial membrane might contribute to the FRET signal, cells expressing Venus-Bcl-XL were transfected with a plasmid encoding mCherry-ActA, a protein that does not bind Bcl-XL but is anchored in the mitochondrial membrane by the ActA tail-anchor sequence (Zhu et al., 1996). Since the BH3 proteins Bim and Bad are also targeted to the outer mitochondrial membrane by C-terminal tail-anchor sequences as

well as by binding to Bcl-XL, the orientation of mCherry-ActA in the membrane should be similar. Expression of mCherry-ActA resulted in a small change in the fluorescence lifetime of Venus-Bcl-XL from approximately 2.90 to 2.76 ns, corresponding to a FLIM FRET efficiency of only 5% (Figure 3C). In the histogram shown, the effect of the FRET between mCherry-ActA and Venus-Bcl-XL is not sufficient to generate two lifetime peaks; rather, it manifests as an asymmetry in the distribution of the measured lifetimes. This result suggests that collisions in the membrane do not contribute significantly to the FRET observed for mCherry-Bad with Venus-Bcl-XL.

As an additional control, FLIM FRET was measured for Venus-Bcl-XL in cells expressing mCherry-Bad2A. As expected, mCherry-Bad2A neither colocalized nor underwent FRET with Venus-Bcl-XL beyond what could be accounted for by collisions (Figure 3D).

Similar experiments performed for the activator BH3-proteins mCherry-tBid (Figure S3A), Bid-mCherry (Figure S3B), and mCherry-BimL (Figure S3C) revealed that both BimL and tBid bound efficiently to Bcl-XL. As expected, Bid-mCherry binding to Venus-Bcl-XL required pretreatment of the cells with TNF-α and cycloheximide to convert the inactive Bid protein to active tBid. Thus, both sensitizer and activator BH3 proteins bind Bcl-XL in live cells.

Taken together, these results suggest that at higher mCherry:Venus ratios a higher proportion of the Venus-Bcl-XL was bound to an mCherry-BH3 protein, decreasing the average fluorescence lifetime of the mitochondrial localized Venus due to FRET with mCherry. This dependence of the decrease in the average fluorescence lifetime of Venus-Bcl-XL on mCherry:Venus ratio allowed us to construct binding curves for the interactions between Venus-Bcl-XL and mCherry-BH3 proteins. However, unlike the studies reported above, in which all of the cellular areas in the images were analyzed, to generate binding curves it was necessary to analyze just areas in the cell enriched in mitochondria. This is because the membrane environment may change the interacting partners of the proteins dramatically (Lovell et al., 2008), and mitochondria are the primary site of apoptosis regulation. Moreover, the higher signal intensities in these regions resulted in more accurate measurements. To generate binding curves, FLIM FRET efficiency (Efficiency %, a measure of the fraction of donor molecules [Venus-Bcl-XL] bound to an acceptor [mCherry-BH3]) was plotted against relative expression (the ratio of Venus to mCherry from intensity-based images).

Binding of mCherry-Bad to either Venus-Bcl-XL or Venus-Bcl-2 in MCF-7 cells generated typical binding curves that saturated in cells expressing relatively high levels of mCherry-Bad, suggesting equilibrium binding (Figures 3E and 3F, black). In contrast, in cells expressing mCherry-ActA and Venus-Bcl-XL, the FLIM FRET efficiency increased linearly with relative expression of mCherry-ActA, indicating that the observed FRET was due to random collisions in the membrane (Figure 3E, red). As expected, binding was not observed in control experiments in which mCherry-Bad2A was expressed in the cells (Figures 3E and 3F, blue). Bad recruitment to mitochondria depends on its binding to Bcl-XL; therefore, cytoplasmic mCherry-Bad2A is expected to collide even less frequently than mCherry-Acta with Venus-Bcl-XL. Similar-shaped binding curves were obtained for mCherry-Bad and mCherry-Bad2A binding to Venus-Bcl-2, demonstrating binding of mCherry-Bad to Venus-Bcl-2 is also saturable and reversible (Figure 3F). It is not possible to compare the values of the FLIM FRET efficiencies obtained for Venus-Bcl-XL with those of Venus-Bcl-2 because they can be affected by alignment of the fluorescent proteins in the heterodimer as well as by differences in the folding fidelity for the two fusion proteins. However, it is possible to use these binding curves to measure the effect of small molecule inhibitors on the binding of BH3-proteins to either antiapoptotic protein.

Mixed-Mode Inhibition of Bcl-XL and Bcl-2 Binding to Bad by ABT-737

When cells expressing Venus-Bcl-XL and mCherry-Bad were treated with ABT-737 for times longer than 4.5 hr (Figure S4), mCherry-Bad redistributed away from Venus-Bcl-XL, consistent with ABT-737 functioning as a Bad mimetic (Figure 4A). Measuring the distribution of lifetimes in the images of ABT-737-treated cells revealed that the average lifetime for Venus-Bcl-XL was 2.80 ns in untransfected cells, while in ABT-737-treated cells expressing mCherry-Bad, the measured fluorescence lifetime was 2.65 ns. The resultant decrease in lifetime gives a calculated FLIM FRET efficiency of 5% in ABT-737-treated cells, demonstrating that the drug effectively inhibited Bad binding to Bcl-XL in live cells.

When FLIM FRET was measured for the mitochondrial regions of >450 cells, we expected to see only a decrease in Emax in the binding curves, as in vitro ABT-737 is a competitive inhibitor for Bad binding to Bcl-XL. Instead we observed changes in both the apparent K_d and Emax, strongly suggesting mixed competitive and noncompetitive inhibition of the interaction between Bad and either Bcl-XL or Bcl-2 by ABT-737 in live cells (Figure 4B). The noncompetitive component is particularly apparent for the affect of ABT-737 on binding of mCherry-Bad to Venus-Bcl-2 (Figure 4C). To examine the effect of ABT-737 in more detail, binding curves were generated for different concentrations of the drug. As expected, increasing the concentration of ABT-737 resulted in commensurately decreased binding of mCherry-Bad to either antiapoptotic protein (Figures 4D and 4E), while the DMSO control had no effect on binding (Figure 4D, black). The changes in K_d caused by ABT-737, indicating noncompetitive inhibition, are particularly evident at higher drug concentrations. These results also demonstrate that FLIM FRET can detect changes in binding from as little as 40 nM ABT-737 and is therefore a very powerful tool for examining protein:protein interactions in live cells.

The BH3 Proteins tBid and Bim Bind Differently to Antiapoptotic Proteins

The interactions of the activator BH3-proteins tBid and Bim with Bcl-XL and Bcl-2 were examined in MCF-7 cells by FLIM FRET (Figure 5). Similar to Bad, tBid binding to both Bcl-XL and Bcl-2 was saturable (Figures 5A and 5B, black) and greatly diminished by the 2A mutation (Figures 5A and 5B, blue). Unfortunately, due to the toxicity of mCherry-tBid when released from Venus-Bcl-XL, there is a lack of points with ratios of mCherry-Venus >1.3. For this reason it was not possible to obtain accurate

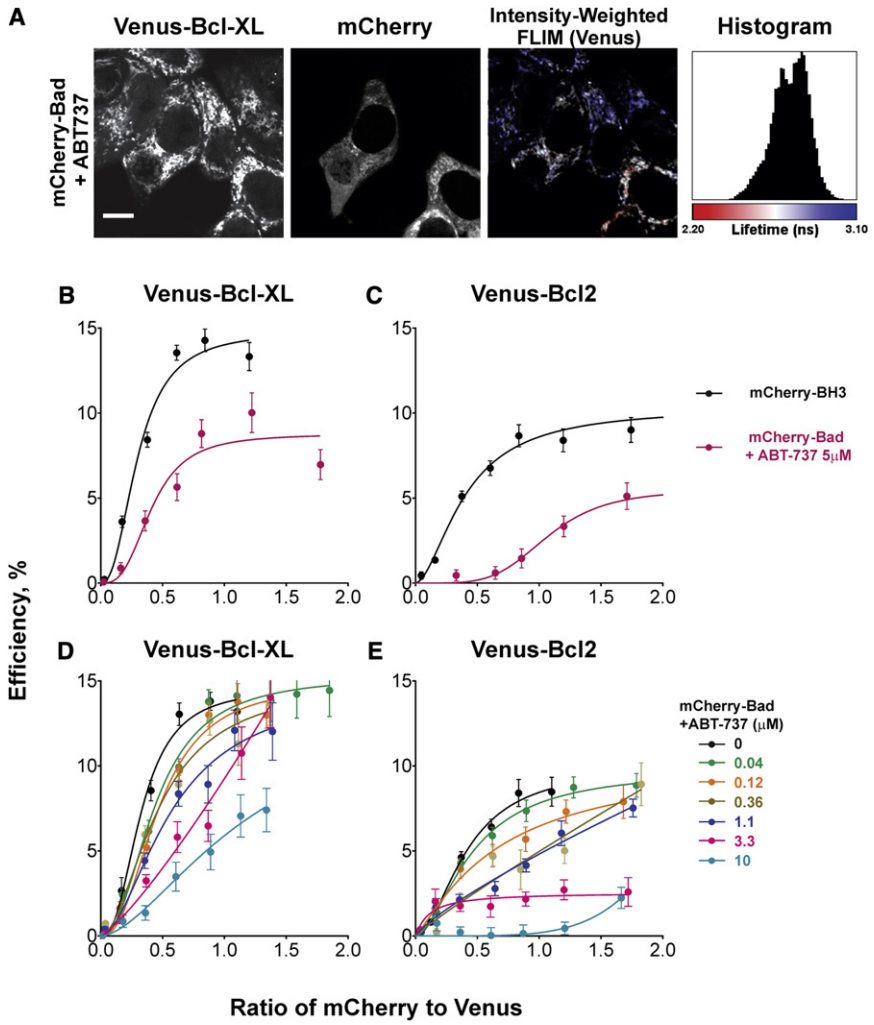

Figure 4. Inhibition of Sensitizer mCherry-Bad Binding to Venus-Bcl-XL and Venus-Bcl-2 by ABT-737 in Live Cells

(A) Intensity images of Venus-Bcl-XL (left) and mCherry (middle) and intensity-weighted FLIM images of Venus-Bcl-XL and pixels intensity histogram (right), as in Figure 3.

(B–E) The FLIM FRET efficiency (Efficiency %) measured for mitochondrial areas in individual cells expressing mCherry-Bad and Venus-Bcl-XL or Venus-Bcl-2 as indicated was plotted versus the ratio of the steady-state intensity of mCherry to Venus fluorescence. Error bars, SE. Each curve > 450 cells. Inhibition of mCherry-Bad binding to Venus-Bcl-XL (B) and Venus-Bcl-2 (C) by ABT-737 shows depressed Emax and increased K_d consistent with mixed mode inhibition (red). The curves for mCherry-Bad without ABT-737 (black) are reproduced from Figures 3E and 3F for comparison. Dose response curves for inhibition of mCherry-Bad binding to Venus-Bcl-XL (D) and Venus-Bcl-2 (E) demonstrate that FLIM FRET can detect changes in binding due to as little as 40 nM ABT-737. The binding curves show dose-dependent changes in Emax and K_d consistent with mixed-mode inhibition. DMSO indicates addition of vehicle only (black) and is equivalent to the curves for mCherry-Bad without ABT-737 (black in B and C). See also Figure S4.

measurements for Emax or K_d for drug-treated cells expressing tBid (Figure 5A, red). However, it is clear that ABT-737 functions at least in part as a competitive inhibitor of tBid binding to Bcl-XL and Bcl-2 (decreased Emax). In cells expressing Venus-Bcl-2, the modest increase in FLIM FRET efficiency detected for drug-treated cells is almost linear with the mCherry/Venus ratio (Figure 5B, red). This result suggests that most of the FRET detected between the two proteins when these cells were treated with ABT-737 resulted from collisions in the outer mitochondrial membrane. Thus, ABT-737 is a very efficient inhibitor of tBid binding to Bcl-2. Taken together, these data are consistent with tBid binding to the antiapoptotic proteins primarily via its BH3 region.

As additional controls, the experiments were repeated using Bid-mCerulean as donor and Venus-Bcl-XL as acceptor (Figure S5). The results obtained fully recapitulated those for Venus-Bcl-XL and Bid-mCherry (Figure S3B). Furthermore, while photobleaching and other control experiments confirmed that most of the change in mCerulean lifetime was due to FRET, binding interactions also reduced the lifetime of the donor (Figure S5). The change due to binding is presumably due to a change in the environment of the donor and contributes to the dynamic range of measurements reported here.

Saturable binding to Bcl-XL and Bcl-2 was also detected for three of the major isoforms of Bim. For mCherry-BimEL or mCherry-BimL, binding to Venus-Bcl-XL saturated at a ratio of mCherry to Venus between 1.0 and 1.5 (Figures 5C–5F). However, for BimS, saturation required ratios of mCherry to Venus greater than 2 (Figures 5G and 5H). This suggests that either BimS does not bind as tightly as the other isoforms of Bim to the antiapoptotic proteins or fusion of mCherry to BimS selectively decreased BimS binding affinity. Given that mCherry-BimS effectively induced apoptosis in MCF-7 cells (Figure S1), the simplest explanation is that BimS does not bind as tightly as the longer Bim isoforms to Venus-Bcl-XL.

To examine the binding interactions in greater detail, we measured the effects of ABT-737 and the 2A mutation on the binding of different Bim isoforms to both antiapoptotic proteins. Unexpectedly, in live MCF-7 cells, ABT-737 had very little effect on the binding of the different Bim isoforms to either Bcl-XL or Bcl-2 (Figures 5C–5H, red). Even for BimS the small change in binding when ABT-737 was added was only evident for mCherry-BimS binding to Venus-Bcl-XL. Inspection of the binding curves suggests that ABT-737 may cause mCherry-BimS binding to saturate at a lower mCherry:Venus ratio (Figures 5G and 5H). Thus, it appears that the drug is largely ineffective at inhibiting binding of at least the longer isoforms of Bim to the antiapoptotic proteins. Consistent with these results, in all three

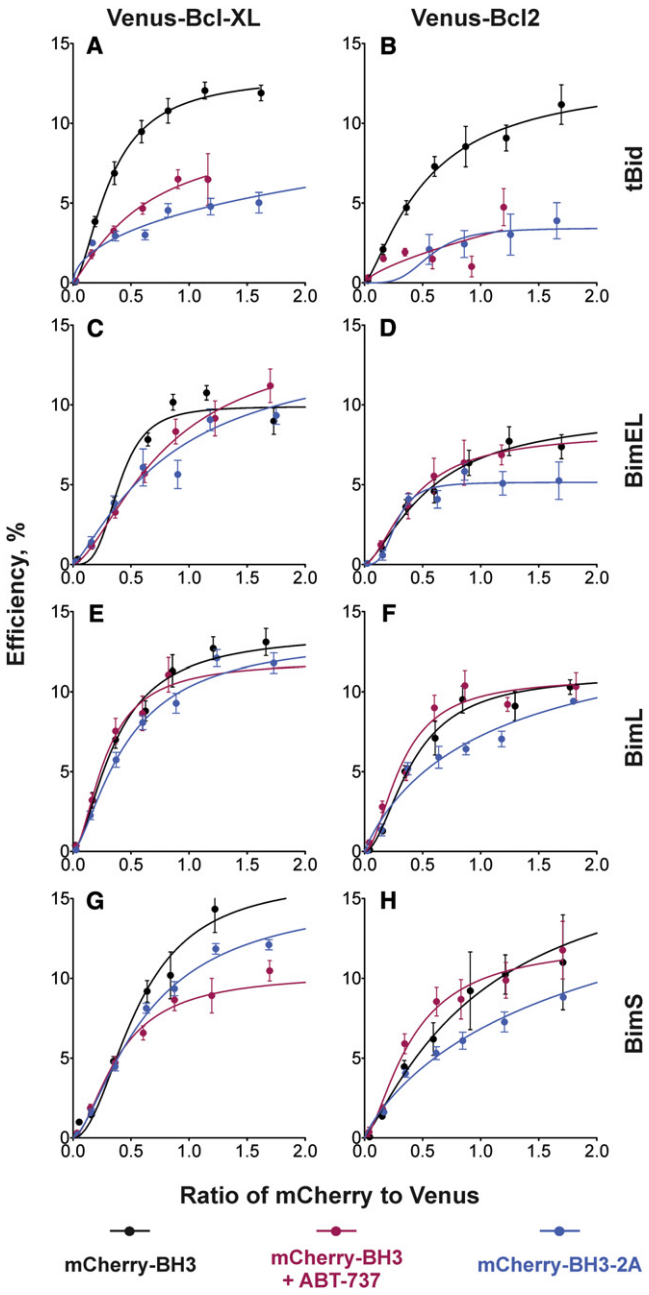

Figure 5. FLIM FRET Binding Curves Reveal that the Activator BH3-Proteins tBid and Bim Bind Differently to Bcl-XL and Bcl-2

(A and B) Binding of mCherry-tBid to Venus-Bcl-XL (A) and Venus-Bcl-2 (B) was saturable (black), inhibited by mutation of the BH3 region (mCherry-tBid2A, blue) and by ABT-737 (red). There are no points for ABT-737-treated cells with mCherry-tBid to Venus-Bcl-XL ratios greater than 1.3 as all of the cells died. The error bars indicate SE and generally increase in size as the number of cells decreased. Each curve represents data from >400 cells.

(C–H) Saturable binding of mCherry-BimEL (C and D), mCherry-BimL (E and F), and mCherry-BimS (G and H) to Venus-Bcl-XL and Venus-Bcl-2 (as indicated) in live cells (black). A small reduction in binding of the BH3 region mutants BimEL2A and BimL2A to Venus-Bcl-2 and of BimS to both Venus-Bcl-XL and Venus-Bcl-2 was detected (blue). ABT-737 did not inhibit BimEL or BimL binding to either Bcl-XL or Bcl-2 (C–F, red). Weak competitive inhibition by ABT-737 of BimS binding to Venus-Bcl-XL but not to Bcl-2 (G and H, red). See also Figure S5.

Bim isoforms the 2A mutations had only a small effect on binding of mCherry-Bim to either antiapoptotic protein (Figures 5C–5H, blue) when compared to the effects of Bad2A (Figures 3E and 3F) and tBid2A (Figures 5A and 5B).

ABT-737 inhibited BimL-induced redistribution of cytoplasmic Venus-Bcl-XL (Figure 2), indicating that the drug inhibited interactions between the proteins in the cytoplasm. Therefore, we speculate that the reason(s) that ABT-737 does not inhibit Bim binding to the antiapoptotic proteins on mitochondria include failure to dissociate preformed complexes between the proteins and additional (non-BH3-mediated) binding interactions between the proteins. These results highlight the importance of examining the binding of full-length BH3 proteins to antiapoptotic proteins in live cells.

Conclusions

Our results demonstrate that in live MCF-7 cells, mCherry fusions to tBid and three isoforms of Bim all elicited apoptosis that was inhibited by Bcl-XL. These results, together with our FLIM FRET data showing that the proteins also bound efficiently to both Venus-Bcl-XL and Venus-Bcl-2 and that mCherry-Bad2A and mCherry-tBid2A did not bind either antiapoptotic protein, suggest that the tagged versions of these Bcl-2 family proteins function similarly to the untagged versions in cells. Moreover, many of the binding interactions we measured in live cells were similar to previous measurements made in vitro. In contrast, for Bim there were very significant differences from previous results using proteins lacking the transmembrane segments (or peptides) in vitro. Our observation that at mitochondria the 2A mutants of all three Bim isoforms bound to both Bcl-XL and Bcl-2 is consistent with inhibition of the retained proapoptotic activities of these mutants by Bcl-XL (Figure S1B). Furthermore, at mitochondria, ABT-737 had no effect on BimL or BimEL and only marginally inhibited the binding of BimS to both antiapoptotic proteins. All of these results for the three Bim isoforms were unexpected based on measurements in vitro (Buron et al., 2010 and reviewed in Leber et al., 2007, 2010).

These differences may be related to our use of full-length proteins, expression in MCF-7 cells, or both. However, the discordance between the binding observed in vitro and what we have measured at mitochondria in live cells is consistent with the observation that the conformations of members of all three subclasses of the Bcl-2 family (antiapoptotic, proapoptotic, and BH3 protein) change with membrane binding. Furthermore, our observation that ABT-737 competes with Bim for binding to Bcl-XL in the cytoplasm (Figure 2B, iv) is consistent with our previous proposal that membrane binding modifies the functional interactions between these proteins, altering the binding affinity of "ligands" and inhibitors (reviewed in Leber et al., 2007, 2010).

Membrane localization may have altered Bim binding to the antiapoptotic proteins in several ways. One explanation for our results is that ABT-737 does not dissociate pre-existing membrane-bound complexes between the Bim isoforms and the antiapoptotic proteins. However, there are other attributes of live cells that may contribute to or predominate in determining the response to ABT-737. Significant published data suggested that Bcl-2 family protein interactions can be regulated by other

cellular events, including posttranslational modifications (reviewed in Puthalakath and Strasser, 2002). Our data do not address the issue of posttranslational modifications, and it is possible that overexpression (as used here) overrides most of these other mechanisms, at least in MCF-7 cells. However, overexpression of mCherry-Bid was neither toxic to cells nor resulted in interactions with Venus-Bcl-XL. Thus, the caspase 8-dependent regulatory mechanism for this protein remained dependent on an exogenous signal (TNF-α and cycloheximide), consistent with the overexpressed protein retaining its normal function.

Colocalization analysis was clearly not sufficient to infer binding. The mCherry-ActA protein showed localization in the outer mitochondrial membrane similar to the mCherry-BH3 proteins, yet our FRET data demonstrated that the interaction of mCherry-ActA with Venus-Bcl-XL was limited to collisions rather than authentic binding. This not only highlights the danger of inferring binding from colocalization data but additionally emphasizes the need for well-constructed control experiments when attempting to quantify protein:protein interactions using FRET.

Furthermore, it was not always possible to visualize ABT-737-mediated dissociation of the BH3-only protein from Bcl-XL or Bcl-2. For example, relocalization was not apparent for tBid bound to Bcl-XL (Figures S3 and S5) or Bcl-2 (not shown). In all cases tBid was efficiently recruited to mitochondria whether expressed directly (mCerulean-tBid and mCherry-tBid) or via TNF-α-induced cleavage of Bid-mCherry. ABT-737 did not change the localization of any of the tBid proteins (Figures S3 and S5) even though it inhibited binding to both antiapoptotic proteins as effectively as mutation of the BH3 region (Figures 5A and 5B). Thus, FLIM FRET is a robust method for quantifying protein:protein interactions in live cells that are difficult to measure other ways.

By generating binding curves for the various proteins, it was possible to examine the molecular mechanism for ABT-737 in live cells. Our results with Bad and tBid strongly suggest that inhibition of binding by ABT-737 is not related to whether the protein functions as a sensitizer or an activator. They also suggest that a major component of ABT-737-mediated inhibition of FLIM FRET is competitive inhibition of binding to the antiapoptotic proteins as expected from the bulk of the previously published data. However, our results demonstrate that in live cells there is also a noncompetitive component to inhibition by ABT-737 that is particularly evident at high drug concentrations.

In contrast, our results suggest that Bim binding may rely on a series of relatively low-affinity interactions that cannot be easily assessed in vitro but that additively have significant impact on binding in live cells. These interactions could include noncanonical interactions in the BH3 region, but as shown above (Figure 5, compare Figure 5C–5F with 5G and 5H), also involve regions found only in the longer Bim isoforms. It remains unknown whether posttranslational modification(s) of the protein are involved. ABT-737 resistance may also depend on the cell type in which the proteins are being measured. Consistent with the latter hypothesis, recently differences have been reported for ABT-737-mediated displacement of Bim from Bcl-2 in different genetic risk groups of multiple myeloma (Bodet et al., 2011). As BimEL is the most commonly expressed isoform, further FLIM FRET analysis of the mechanism by which this protein binds to antiapoptotic proteins will be important to guide development of new small molecules as potential anticancer agents. Furthermore, FLIM FRET is likely to be a useful tool to guide the further development of other drugs targeting protein:protein interactions in cells.

EXPERIMENTAL PROCEDURES

Constructs

Plasmids encoding the Venus, mCerulean, or mCherry fluorescence proteins in place of the EGFP coding region in pEGFP-C1 (Clontech) were a kind gift from Ray Truant (McMaster University). To generate plasmids encoding the fusion proteins, the required coding regions were amplified by PCR and inserted into the plasmids encoding the appropriate fluorescence protein. Plasmids encoding mCerulean-ActA and mCherry-ActA were prepared by replacing the Bcl-2 coding region from a plasmid encoding Bcl2-ActA (Zhu et al., 1996) with PCR product coding for the fluorescence proteins. All of the plasmids included coding sequences for a GGS linker sequence between the coding regions except for mCherry-Bad (linker sequence, SGLRSRGG).

Steady-State Fluorescence Confocal Imaging

Steady-state fluorescence images were acquired as described in the Supplemental Experimental Procedures using a Leica TCS SP5. Images of mCerulean, Venus, and mCherry were acquired using 458 nm, 514 nm, and 561 nm excitation, respectively, and emission was collected between 465–495 nm, 525–555 nm, and 580–670 nm, respectively. The average fluorescence intensity of individual cells or regions was quantified using ImageJ. MitoTracker Deep Red (MTDR) images were acquired with 633 nm excitation and 650–720 nm emission. Images of lissamine rhodamine-labeled antibodies used to detect cytochrome *c* were obtained by illumination with a 561 nm laser and detecting emission between 575–680 nm.

Fluorescence Lifetime Measurements

Fluorescence lifetimes were quantified by time-correlated single-photon counting (TCSPC) as described in the Supplemental Experimental Procedures. TCSPC images were acquired with a Leica TCS SP5 confocal microscope (Leica Microsystems CMS GmbH, Mannheim, Germany) equipped with an integrated SPC-830 TCSPC system (Becker and Hickl GmbH, Berlin, Germany) and Chameleon Ultra pulsed laser (Coherent Inc.).

The processed lifetime images were exported, and ImageJ was used to generate lifetime histograms and to quantify the average fluorescence lifetime of individual cells or mitochondrial regions. Fluorescence lifetime images are presented in a continuous pseudocolor scale ranging from 2.2 to 3.1 ns. Intensity-weighted fluorescence lifetime images were generated using ImageJ.

SUPPLEMENTAL INFORMATION

Supplemental Information includes five figures and Supplemental Experimental Procedures and can be found with this article online at doi:10.1016/j.molcel.2012.01.030.

ACKNOWLEDGMENTS

This work was supported by grant FRN12517 from the Canadian Institute of Health Research (CIHR) to D.W.A. and B.L. and by a Tier I Canada Research Chair in Membrane Biogenesis to D.W.A. Q.L. is recipient of a postdoctoral fellowship from the Canadian Breast Cancer Foundation, Ontario Division. The authors thank Dr. Ray Truant for supplying plasmids encoding fluorescence proteins and Dr. Alba Guarne for helpful review of the manuscript.

Received: March 22, 2011
Revised: October 23, 2011
Accepted: January 12, 2012
Published online: March 29, 2012

REFERENCES

Billen, L.P., Kokoski, C.L., Lovell, J.F., Leber, B., and Andrews, D.W. (2008). Bcl-XL inhibits membrane permeabilization by competing with Bax. PLoS Biol. *6*, e147.

Bodet, L., Gomez-Bougie, P., Touzeau, C., Dousset, C., Descamps, G., Maïga, S., Avet-Loiseau, H., Bataille, R., Moreau, P., Le Gouill, S., et al. (2011). ABT-737 is highly effective against molecular subgroups of multiple myeloma. Blood *118*, 3901–3910.

Bouillet, P., Metcalf, D., Huang, D.C.S., Tarlinton, D.M., Kay, T.W.H., Köntgen, F., Adams, J.M., and Strasser, A. (1999). Proapoptotic Bcl-2 relative Bim required for certain apoptotic responses, leukocyte homeostasis, and to preclude autoimmunity. Science *286*, 1735–1738.

Bruncko, M., Oost, T.K., Belli, B.A., Ding, H., Joseph, M.K., Kunzer, A., Martineau, D., McClellan, W.J., Mitten, M., Ng, S.C., et al. (2007). Studies leading to potent, dual inhibitors of Bcl-2 and Bcl-xL. J. Med. Chem. *50*, 641–662.

Buron, N., Porceddu, M., Brabant, M., Desgué, D., Racoeur, C., Lassalle, M., Péchoux, C., Rustin, P., Jacotot, E., and Borgne-Sanchez, A. (2010). Use of human cancer cell lines mitochondria to explore the mechanisms of BH3 peptides and ABT-737-induced mitochondrial membrane permeabilization. PLoS ONE *5*, e9924.

Certo, M., Del Gaizo Moore, V., Nishino, M., Wei, G., Korsmeyer, S., Armstrong, S.A., and Letai, A. (2006). Mitochondria primed by death signals determine cellular addiction to antiapoptotic BCL-2 family members. Cancer Cell *9*, 351–365.

Chauhan, D., Velankar, M., Brahmandam, M., Hideshima, T., Podar, K., Richardson, P., Schlossman, R., Ghobrial, I., Raje, N., Munshi, N., and Anderson, K.C. (2007). A novel Bcl-2/Bcl-X(L)/Bcl-w inhibitor ABT-737 as therapy in multiple myeloma. Oncogene *26*, 2374–2380.

Chen, Y., and Periasamy, A. (2004). Characterization of two-photon excitation fluorescence lifetime imaging microscopy for protein localization. Microsc. Res. Tech. *63*, 72–80.

Chen, Y., Mills, J.D., and Periasamy, A. (2003). Protein localization in living cells and tissues using FRET and FLIM. Differentiation *71*, 528–541.

Chen, L., Willis, S.N., Wei, A., Smith, B.J., Fletcher, J.I., Hinds, M.G., Colman, P.M., Day, C.L., Adams, J.M., and Huang, D.C. (2005). Differential targeting of prosurvival Bcl-2 proteins by their BH3-only ligands allows complementary apoptotic function. Mol. Cell *17*, 393–403.

Galluzzi, L., Aaronson, S.A., Abrams, J., Alnemri, E.S., Andrews, D.W., Baehrecke, E.H., Bazan, N.G., Blagosklonny, M.V., Blomgren, K., Borner, C., et al. (2009). Guidelines for the use and interpretation of assays for monitoring cell death in higher eukaryotes. Cell Death Differ. *16*, 1093–1107.

Giam, M., Huang, D.C., and Bouillet, P. (2008). BH3-proteins and their roles in programmed cell death. Oncogene *27*, S128–S136.

Hann, C.L., Daniel, V.C., Sugar, E.A., Dobromilskaya, I., Murphy, S.C., Cope, L., Lin, X., Hierman, J.S., Wilburn, D.L., Watkins, D.N., and Rudin, C.M. (2008). Therapeutic efficacy of ABT-737, a selective inhibitor of BCL-2, in small cell lung cancer. Cancer Res. *68*, 2321–2328.

Hsu, Y.T., and Youle, R.J. (1998). Bax in murine thymus is a soluble monomeric protein that displays differential detergent-induced conformations. J. Biol. Chem. *273*, 10777–10783.

Kirkin, V., Joos, S., and Zörnig, M. (2004). The role of Bcl-2 family members in tumorigenesis. Biochim. Biophys. Acta *1644*, 229–249.

Leber, B., Lin, J., and Andrews, D.W. (2007). Embedded together: the life and death consequences of interaction of the Bcl-2 family with membranes. Apoptosis *12*, 897–911.

Leber, B., Lin, J., and Andrews, D.W. (2010). Still embedded together binding to membranes regulates Bcl-2 protein interactions. Oncogene *29*, 5221–5230.

Lee, E.F., Czabotar, P.E., van Delft, M.F., Michalak, E.M., Boyle, M.J., Willis, S.N., Puthalakath, H., Bouillet, P., Colman, P.M., Huang, D.C., and Fairlie, W.D. (2008). A novel BH3 ligand that selectively targets Mcl-1 reveals that apoptosis can proceed without Mcl-1 degradation. J. Cell Biol. *180*, 341–355.

Lovell, J.F., Billen, L.P., Bindner, S., Shamas-Din, A., Fradin, C., Leber, B., and Andrews, D.W. (2008). Membrane binding by tBid initiates an ordered series of events culminating in membrane permeabilization by Bax. Cell *135*, 1074–1084.

Mason, K.D., Vandenberg, C.J., Scott, C.L., Wei, A.H., Cory, S., Huang, D.C., and Roberts, A.W. (2008). *In vivo* efficacy of the Bcl-2 antagonist ABT-737 against aggressive Myc-driven lymphomas. Proc. Natl. Acad. Sci. USA *105*, 17961–17966.

O'Connor, L., Strasser, A., O'Reilly, L.A., Hausmann, G., Adams, J.M., Cory, S., and Huang, D.C. (1998). Bim: a novel member of the Bcl-2 family that promotes apoptosis. EMBO J. *17*, 384–395.

Oltersdorf, T., Elmore, S.W., Shoemaker, A.R., Armstrong, R.C., Augeri, D.J., Belli, B.A., Bruncko, M., Deckwerth, T.L., Dinges, J., Hajduk, P.J., et al. (2005). An inhibitor of Bcl-2 family proteins induces regression of solid tumours. Nature *435*, 677–681.

Peng, J., Tan, C., Roberts, G.J., Nikolaeva, O., Zhang, Z., Lapolla, S.M., Primorac, S., Andrews, D.W., and Lin, J. (2006). tBid elicits a conformational alteration in membrane-bound Bcl-2 such that it inhibits Bax pore formation. J. Biol. Chem. *281*, 35802–35811.

Periasamy, A., and Day, R.N. (2005). Molecular Imaging, FRET Microscopy and Spectroscopy (Oxford: Oxford University Press).

Puthalakath, H., and Strasser, A. (2002). Keeping killers on a tight leash: transcriptional and post-translational control of the pro-apoptotic activity of BH3-proteins. Cell Death Differ. *9*, 505–512.

Renton, J.P., Xu, N., Clark, J.J., and Hansen, M.R. (2010). Interaction of neurotrophin signaling with Bcl-2 localized to the mitochondria and endoplasmic reticulum on spiral ganglion neuron survival and neurite growth. J. Neurosci. Res. *88*, 2239–2251.

Schimmer, A.D., Hedley, D.W., Chow, S., Pham, N.A., Chakrabartty, A., Bouchard, D., Mak, T.W., Trus, M.R., and Minden, M.D. (2001). The BH3 domain of BAD fused to the Antennapedia peptide induces apoptosis via its alpha helical structure and independent of Bcl-2. Cell Death Differ. *8*, 725–733.

Shaner, N.C., Campbell, R.E., Steinbach, P.A., Giepmans, B.N., Palmer, A.E., and Tsien, R.Y. (2004). Improved monomeric red, orange and yellow fluorescent proteins derived from Discosoma sp. red fluorescent protein. Nat. Biotechnol. *22*, 1567–1572.

Vogler, M., Weber, K., Dinsdale, D., Schmitz, I., Schulze-Osthoff, K., Dyer, M.J., and Cohen, G.M. (2009). Different forms of cell death induced by putative BCL2 inhibitors. Cell Death Differ. *16*, 1030–1039.

Wang, K., Yin, X.M., Chao, D.T., Milliman, C.L., and Korsmeyer, S.J. (1996). BID: a novel BH3 domain-only death agonist. Genes Dev. *10*, 2859–2869.

Yang, E., Zha, J., Jockel, J., Boise, L.H., Thompson, C.B., and Korsmeyer, S.J. (1995). Bad, a heterodimeric partner for Bcl-XL and Bcl-2, displaces Bax and promotes cell death. Cell *80*, 285–291.

Youle, R.J., and Strasser, A. (2008). The BCL-2 protein family: opposing activities that mediate cell death. Nat. Rev. Mol. Cell Biol. *9*, 47–59.

Zacharias, D.A., Violin, J.D., Newton, A.C., and Tsien, R.Y. (2002). Partitioning of lipid-modified monomeric GFPs into membrane microdomains of live cells. Science *296*, 913–916.

Zhu, W., Cowie, A., Wasfy, G.W., Penn, L.Z., Leber, B., and Andrews, D.W. (1996). Bcl-2 mutants with restricted subcellular location reveal spatially distinct pathways for apoptosis in different cell types. EMBO J. *15*, 4130–4141.